Electrochemical State-Based Sinusoidal Ripple Current Charging Control

Yong-Duk Lee, *Student Member, IEEE*, and Sung-Yeul Park, *Member, IEEE*

***Abstract*—This paper presents a sinusoidal ripple current charging algorithm based on embedded impedance measurements. Existing battery charging strategies typically do not take into account the electrochemical properties of batteries, because these factors are difficult to obtain during charging operation. Factors of concern include lithium plating, growth of a solid electrolyte interphase, limited exchange current, and slow diffusion rates. It is beneficial to utilize these parameters during charging operation, because the charging current can adapt to the time-varying characteristics of a battery. Consequently, battery life cycle, charging speed, and charging efficiency all improve. In this paper, rigorous analysis of electrochemical characteristics is performed and a method for minimization of variations of charge transfer impedance is explained based on a sinusoidal ripple current charging algorithm. To obtain the optimal ripple current frequency, ac impedance analysis based on the *dq* transformation method is proposed. As a result, this method improved charging efficiency and reduced lithium plating by activation polarization. Simulation and experimental results using a 14.6-V $LiFeMgPO_4$ battery are used to validate and demonstrate the performance of the proposed control scheme. Based on the proposed control scheme, the charging time and efficiency of the Li-ion battery are improved by 5.1% and 5.6%, respectively.**

***Index Terms*—Battery chargers, frequency control, impedance measurement.**

I. Introduction

WHY are investments of money and research in batteries increasing exponentially? The demand for high-performance rechargeable batteries is rapidly growing for the following industries: 1) Automotive, 2) military, 3) mobile, 4) medical instrumentation, 5) industrial device manufacturing, 6) back-up power supplies, 7) aerospace technologies, and 8) renewable energy source support. Due to these demands, the market is growing and appears very promising. Although the demand is growing, the expansion of rechargeable batteries into new applications becomes increasingly problematic. In these applications, fast charging, long life cycle, and efficient charging are all key considerations. Significant research has been conducted on the reduction of charging time while incurring low charging losses. The former considerations are intimately related to charging efficiency; if we can achieve high-charging efficiency, a long life cycle can be obtained as well [1], [2]; however, it is difficult to achieve both fast-charging and high-charging efficiency at the same time and this remains a challenge.

Short life cycle and long charging time are the results of serious problems such as increased heat losses, maximum capacity reduction, and short circuiting. Additionally, formation of a solid electrolyte interphase (SEI) is a rather severe problem, because it can minimize the available range of the open-circuit voltage curve [3], [4]. Typically, the causes of short life cycle and long charging time are lithium plating and growth of a SEI by polarization effects [4]–[6]. By definition, polarization occurs when Li+ ions are deposited on the surface of the anode. This is influenced in regard to the kinetics of local electron activity, interface overpotential, and current density. Usually, lithium plating propagates overpotential at the interface between the electrolyte and electrode. Thus, internally, lithium plating results in reduced diffusion rate and reduced ion conductivity [7]–[10].

Ion transportation in a battery is commonly encouraged by heat balancing and addition of catalytic solution. These corrective methods are effective, but are only applicable in a laboratory environment and are simply not feasible at an application level. Therefore, a solution from the perspective of the electrical engineer is required for real applications.

In finding this solution, detecting the beginning point of lithium plating is critical in charging adaptation. Typically, in charging and discharging phases, it is detectable when:

1) lithium plating causes a change in anode overpotential;
2) lithium plating causes a change in the internal resistance;
3) lithium plating causes changes in concentration and activation polarizations.

From the electrical engineer's perspective, the resistance's varying behavior is the most important observation amongst the three indications of lithium plating, because battery impedance is relatively easy to measure. In order to utilize the resistance of a battery, the relationship between the internal resistance behavior and phenomena of electrochemical factors must be elucidated, shown in Fig. 1. At the point, *t1* of Fig. 1(a), the anode is polarized with activated Li+. As a result, the anode potential becomes negative [7], [8] and the internal resistance is then saturated. Negative overpotential is interpreted as a hindrance factor in terms of the charging curve, because the terminal voltage can be calculated simply by the difference in potential between the cathode and the anode. Thus, the saturation point of the internal resistance can be utilized for new battery charging algorithms. In addition, this relation can be described by the conductivity and concentration plot, shown in Fig. 1(b). At some concentration of Li+, the conductivity becomes either saturated or degraded [11]. This limitation or reduction of conductivity is the result of negative overpotential and saturated/increased internal resistance, respectively [8], [12]–[16]. This indicates that

Manuscript received April 9, 2014; revised June 26, 2014; accepted August 14, 2014. Date of publication September 4, 2014; date of current version March 5, 2015. Recommended for publication by Associate Editor S. Choi

The authors are with the Department of Electrical and Computer Engineering, University of Connecticut, Storrs, CT 06269-4157 USA (e-mail: yongduk@engr.uconn.edu; supark@engr.uconn.edu).

Color versions of one or more of the figures in this paper are available online at http://ieeexplore.ieee.org.

Digital Object Identifier 10.1109/TPEL.2014.2354013

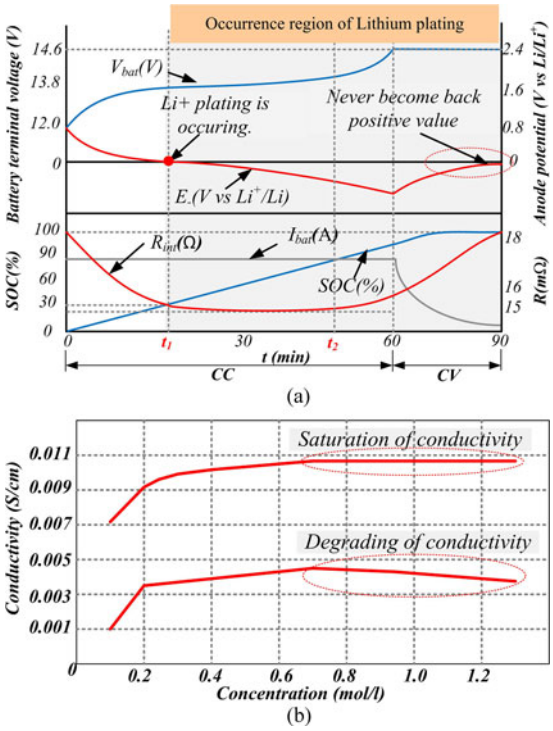

Fig. 1. Lithium plating beginning point and its phenomena: (a) The anode potential and internal resistance in CCCV charging [8, 12–16] and (b) a relationship between concentration and conductivity [11].

the conductivity is related to both the resistance and the internal potential difference.

Traditional charging methods such as float charging, trickle charging, constant voltage, constant current (CC), and constant power have many of their own merits as follows:

1) low-cost implementation;
2) self-discharge compensation and strict overvoltage safety;
3) convenience of operation.

However, these methods suffer from the aforementioned problems, because conventional charging methods omit electrochemical processes occurring within a battery. Typically, lithium plating occurs throughout a constant current constant voltage (CCCV) charge, especially at high currents and low temperatures. As a result, lithium plating and a SEI at the anode interface reduces the charging capacity [16]–[18].

Attempts to utilize electrochemical factors as a basis for charging control has been widely investigated, and techniques such as intelligent charging using a neural network [19], optimization and multistage charging [20]–[22], fuzzy control [23], model predictive control [24], pulse charging [25], [26], sinusoidal charging [27], [28], boost charging [29], and resistance compensation [30], [31] have been created. Most intelligent chargers seek to characterize the nonlinear relationship between a battery's temperature, voltage, and charging current. Amongst the intelligent charging methods, the most remarkable solutions are pulse charging and sinusoidal ripple current charging. These charging algorithms may feature rest periods and depolarization pulses, which mitigate both overpotential and polarization occurring due to lithium plating [32], [33]. In addition, sinusoidal charging uses an optimal frequency to minimize battery impedance and losses. This technique also follows a depolarization effect for minimizing lithium plating. These methods are documented in many papers and are proven to reduce the charging time and other deleterious effects [25], [26], [32]–[34]. However, there is a lack of detailed analysis and methods for obtaining parameters for pulse charging and sinusoidal charging with respect to all of the aforementioned electrochemical considerations. In addition, in the studies on sinusoidal ripple current charging, the impact of the magnitude of the dc current is not considered.

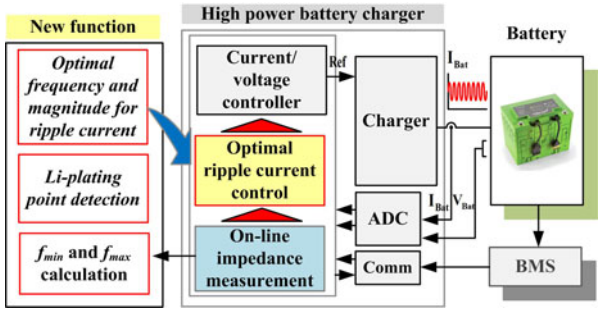

Fig. 2. Block diagram of proposed charging algorithm.

In this paper, we propose an advanced sinusoidal ripple current charging with an embedded impedance measurement, shown in Fig. 2. The proposed method will provide an adaptive online charging algorithm with respect to a battery's electrochemical state. The optimal sinusoidal frequency and magnitude will be determined as a result of the online impedance measurement performed by the battery charger. Determination of the optimal frequency range of the ripple current and reasonable dc current magnitude levels are analyzed and the algorithm used to control these two factors is applied in the digital control system of the charger. To implement the optimal ripple current frequency, an ac impedance analysis method based on the *dq* transformation is used.

II. Analysis of Lithium Plating

A. Review of Basic Electrochemical Fundamentals

A difference in chemical potentials between the two electrodes results in the transfer of lithium ions from the cathode to the anode through the electrolyte solution [35], [36]. In order to better understand the electrochemical phenomenon, an equivalent circuit model is used. Three major mechanisms are considered in this analysis: the mass transfer effect, the charge transfer effect, and the ohmic effect [35]–[37]. An electrochemical battery model can be represented by an equivalent circuit consisting of passive components as follows: (1) the diffusion as a result of the concentration polarization, Z_W (Warburg impedance), (2) the activation polarization factors, $R_{\rm CT}$ and $C_{\rm DL}$, and (3) the ohmic resistance, R_O. In addition, the parasitic inductance, L_e, which is a product of external/internal connections, can be included in the model. Concentration polarization is represented by Warburg impedance. The ions are transported by diffusion and migration. The area of contact between the electrode and

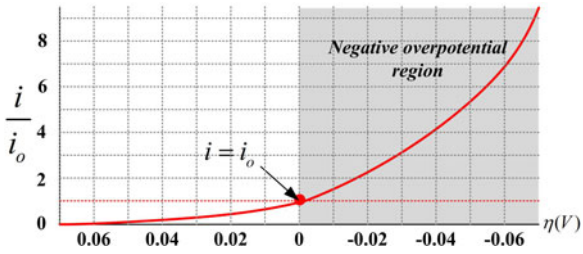

Fig. 3. Exchange current rate vs over-potential [11].

the electrolyte forms the charge zone for the activation polarization. It is modeled as R_{CT}, which determines the rate of the exchange current with the double-layer capacitance in parallel. The electrolyte resistance is modeled based on the conductivity of the electrolyte.

B. Analysis of Overpotential by Lithium Plating

The kinetics of overpotential can be explained by the Butler–Volmer equation and the Nernst equation as follows [38]:

$$i = i_o \frac{nF\eta}{RT} \tag{1}$$

where i is the applied current, i_o is the exchange current density, n is the number of electrons participating in the electrode reaction, η is the overpotential, F is the Faraday constant, R is the gas constant, and T is the temperature (K). Since the overpotential depends on charge transfer resistance, R_{CT}, (1) can be simplified

$$\eta \approx \frac{RT}{nFi_o} i = R_{\mathrm{CT}} i, \quad R_{\mathrm{CT}} = \frac{RT}{nFi_o}. \tag{2}$$

These two (1) and (2) describe the relationship with respect to the applied charging current, exchange current by R_{CT} and the overpotential. Basically, the exchange current, i_o, depends on the charge transfer resistance, which changes as other internal conditions change during the course of charging/discharging.

In addition, the negative overpotential due to lithium plating is caused by the ratio of the exchange current and applied current. Usually, Fig. 3 is used to explain this relationship. Negative overpotential occurs when the applied current is greater than the exchange current. Therefore, the lithium plating can be affected by the charge transfer resistance and applied current. Conversely, in order to obtain the optimal charging condition, the applied current should match the exchange current, whenever the charge transfer resistance has changed.

III. Analysis of Ripple Current and Pulse Charging Methods

In general, ac ripple current is superposed with dc current, which precipitates self-heating. Thus, ripple currents of any frequency contribute to loss factors related to heat. Through the Fourier series, this relationship can be easily proved. Fig. 4 shows the Fourier series and the waveforms between dc CC and ac ripple current charging methods. The ripple current is always larger than the dc current. This means that losses due to the ripple current are larger than that of the dc current. The

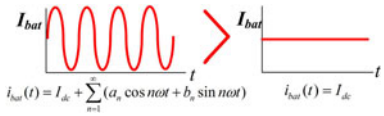

Fig. 4. Charging current with ripple current and dc charging current.

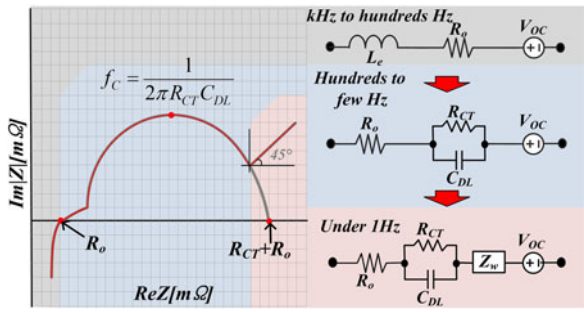

Fig. 5. Impedance change with respect to frequency.

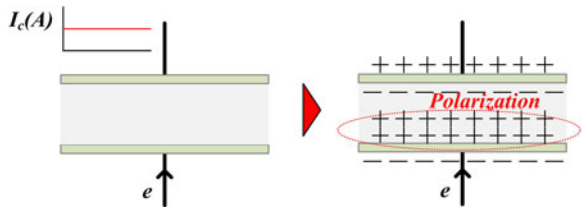

Fig. 6. Polarization mechanism of double layer capacitor.

benefits of ripple current charging have been published in [27] and [28]. According to their proposed methods, charging at the optimal ripple current frequency can reduce the charging time and improve the charging efficiency, because, at the optimal frequency, the ac impedance of a battery can be minimized. This method is based on electrochemical impedance spectroscopy analysis of the equivalent circuit of a battery.

From the impedance spectrum, it is possible to deduce the equivalent circuit and the minimum point of the ac impedance of a battery can be easily found, shown in Fig. 5. At a certain frequency within the kilohertz and hundreds of hertz range, the total impedance is equal to the electrolyte resistance, R_O, because C_{DL} and Z_w become negligibly small. Namely, at the boundary frequency between the inductive and capacitive regions, battery impedance can be minimized. If a low-frequency range is used, the losses can be increased because of the charge transfer resistance and Warburg impedance.

Even if the frequency of the ripple current is reasonably controlled, dc current is still a component of the charging current. Theoretically, the minimized resistance affects only ac ripple voltage and current in electrical theory. However, electrochemical phenomena differ from electrical behavior. Therefore, verification of the effects of dc charging current is required.

In order to validate the effects of dc charging current with sinusoidal ripple current, it is necessary to understand the physical characteristics of the double-layer capacitance by activation polarization. These mechanisms are related to charge transfer and

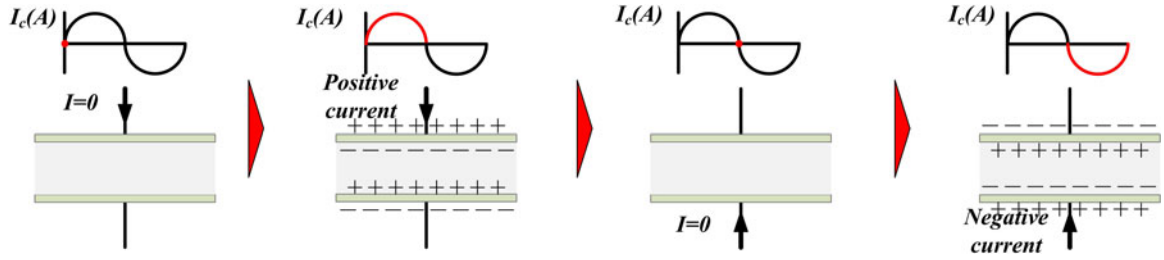

Fig. 7. Operation of ac ripple current.

conductivity. Principally, the charging process of the double-layer capacitance involves Faradaic charge-transfer processes [39], [40]. This process is rather similar to the charging process of a capacitor. From applied dc current, the double-layer capacitance becomes charged to the voltage, $V_{\text{double\_layer}}$, by the applied current and charge transfer resistance as follows:

$$V_{\text{double\_layer}} = R_{\text{CT}} i. \tag{3}$$

At this time, the current flows into the capacitor. Subsequently, the entirety of the applied current flows through the charge transfer resistance, R_{CT}. After the double-layer capacitance, C_{DL}, has been charged, dc charging current magnitude is maintained and dc current does not flow through C_{DL}. In this case, positive charges will accumulate on the negative electrode shown in Fig. 6. The conductivity is reduced, due to the resulting plating and polarization [38], [39].

In order to solve this problem, ac current injection is an effective method, because ac current changes polarity twice in one period, shown in Fig. 7. As a result, concentration polarization in electrodes is minimized because charge accumulation is reduced. In the *RC* parallel configuration of the charge transfer reaction, the injection of ripple current can be helpful for reduction of the concentration polarization. This validates the effectiveness of pulse and sinusoidal ripple current charging.

A method for avoiding lithium plating is derived by explaining the polarization of the double layer. However, ascertaining the optimal frequency is not yet apparent, though it is necessary to prevent positive charge accumulation. Typically, the optimal frequency value is related to the time constant of *RC* parallel circuit in the equivalent circuit of the battery. The time constant is

$$\tau = R_{\text{CT}} C_{\text{DL}}. \tag{4}$$

Typically, at 1τ, C_{DL} is not fully charged. This means that if the input current has a higher frequency than the time constant, the charge transfer rate does not worsen. It can be described by this relationship

$$f_{\text{optimal\_frequency}} > \frac{1}{2\pi R_{\text{CT}} C_{\text{DL}}}. \tag{5}$$

Thus, (5) represents the minimum frequency to prevent charge accumulation.

According to our hypothesis, the frequency of the sinusoidal ripple current ranges from the boundary condition between predominant capacitance and inductance to the time-constant frequency. Now, not only is ripple current charging validated for ac resistance minimization, but also the accumulation of positive charges due to the dc current component can be minimized. Thus, the ripple current in this frequency range can minimize overpotential regarding activation polarization, which affects the double-layer capacitance.

In addition, the rest period has a role in relaxing the concentration gradient. The optimal magnitude of the ripple current is also of interest. Therefore, the next step is to decide the proper magnitude of the ac ripple current.

Basically, the charge, Q, is defined as follows:

$$Q = C_{\text{DL}} V_{\text{over\_potential}}. \tag{6}$$

And the current of the double-layer capacitance, i_{CDL}, is

$$i_{C_{\text{DL}}} = C_{\text{DL}} \frac{dV_{\text{over\_potential}}}{dt}. \tag{7}$$

From (6) and (7), the charge, Q, can be defined as

$$Q = i_{C_{\text{DL}}} \frac{dt}{dV_{\text{over\_potential}}} V_{\text{over\_potential}}. \tag{8}$$

From the defined optimal frequency (5), the charging time (4) is used. At τ, the charge, Q, is determined by considering voltage across the *RC* parallel circuit

$$Q = i_{C_{\text{DL}}} R_{\text{CT}} C_{\text{DL}}. \tag{9}$$

At τ, the minimum magnitude of the double-layer capacitance current can be calculated as

$$i_{C_{\text{DL}}} = \frac{C_{\text{DL}} R_{\text{CT}} I_{\text{bat}} e^{-1}}{R_{\text{CT}} C_{\text{DL}}} = I_{\text{bat}} e^{-1}. \tag{10}$$

Therefore, by investigating the plating effects in the double-layer capacitance, the minimum frequency and magnitude can be determined as follows:

$$i_{C_{\text{DL}}} = I_{\text{bat}} e^{-1}, f_{\text{optimal\_frequency}} > \frac{1}{2\pi R_{\text{CT}} C_{\text{DL}}}. \tag{11}$$

In addition, in order to avoid excessive peak current from the charger, the maximum current magnitude is required. This value is related to the time constant, which indicates the time it takes to charge/discharge the capacitor to one half. Thus, the factor that governs how quickly the charge drops is achieved through the charge resistance. This relationship is

$$t_{1/2} = \tau \ln(2). \tag{12}$$

Therefore, the charge transfer current and double-layer current is the same at a certain point in time. This point is usually the half-way point of the exponential current, because the charging and discharging rates are the same. Therefore, the maximum

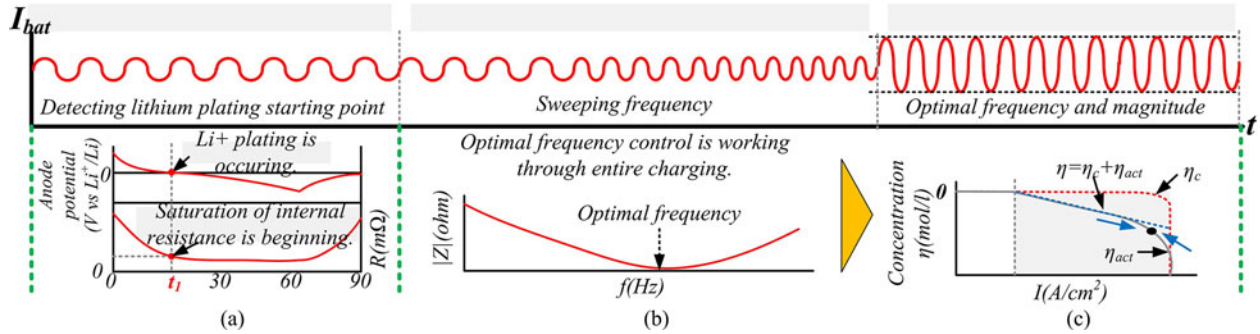

Fig. 8. Proposed charging strategy.

ripple current magnitude can be one half of the dc component of the battery current.

IV. Proposed Charging Strategy

A. Processes of the Proposed Charging Strategy

In Fig. 8, the charging strategy for ac ripple current charging is proposed with three sequences as follows:

1) sequence one: detection of the beginning of lithium plating;
2) sequence two: optimal frequency detection by sweeping the ac current frequency;
3) sequence three: application of the optimal frequency and magnitude ripple current and continual tracking of the optimal frequency.

The first sequence is meant to detect the starting point of lithium plating. Since this point relies on the charge rate, it is not easy to determine. In this paper, to evaluate the starting point, the real part of the impedance is monitored used during the charging process. As explained in the introduction, the internal impedance is related to the conductivity and the lithium plating. Fig. 8(a) shows the relationship between the real part of the impedance and the lithium plating beginning point. When negative overpotential occurs, lithium plating occurs and the real part of the impedance becomes saturated. Therefore, by evaluating the saturation point of the real part of the impedance, the beginning point of lithium plating can be estimated.

The second sequence is for detection of the optimal frequency by sweeping the ac current frequency, shown in Fig. 8(b). From this frequency sweep, we can obtain important information such as (1) the moderate frequency, (2) the real and imaginary parts of the impedance, (3) R_o, (4) $R_{\rm CT}$, and (5) $C_{\rm DL}$. The moderate frequency indicates the minimum frequency of the ripple current. At minimum imaginary impedance, the ohmic resistance, R_o, and the maximum frequency of the sinusoidal ripple current are defined. Therefore, the optimal frequency range can be ascertained from this process.

The final step is to apply the optimal magnitude and frequency references to the charging current shown in Fig. 8(c). The optimal magnitude is calculated by

$$I_{C-\rm rate}e^{-1} \le M \le \frac{I_{C-\rm rate}}{2} \tag{13}$$

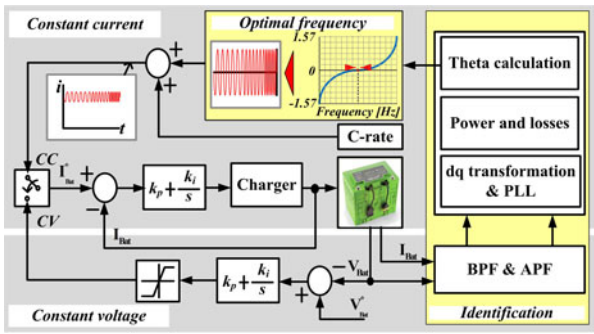

Fig. 9. Control block of proposed system.

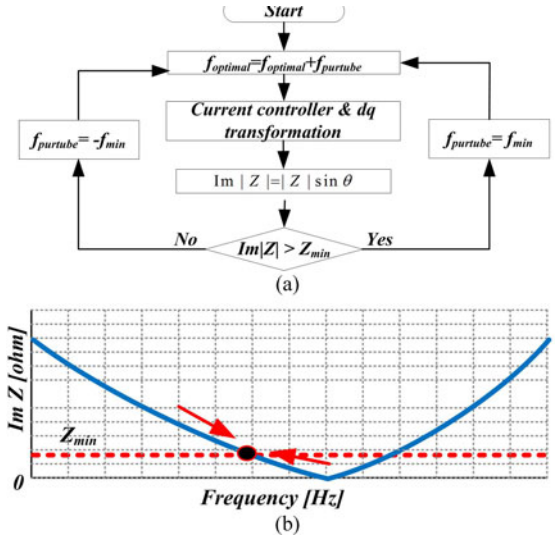

Fig. 10. Controller operation: (a) flow chart and (b) frequency control method.

where $I_{C-\rm rate}$ is the magnitude of the dc charging current. In this paper, a magnitude of $(I_{C-\rm rate}/2)$ with $1/\tau$ is applied. It is notable that the optimal frequency point will change throughout the charging process, so the proposed optimal frequency controller tracks this point continuously.

B. Ripple Current Frequency Sweeping and Battery Impedance Measurement

Fig. 9 shows the control block diagrams of both the optimal frequency controller, which operates in regard to the online measured impedance and the converter controller. The converter

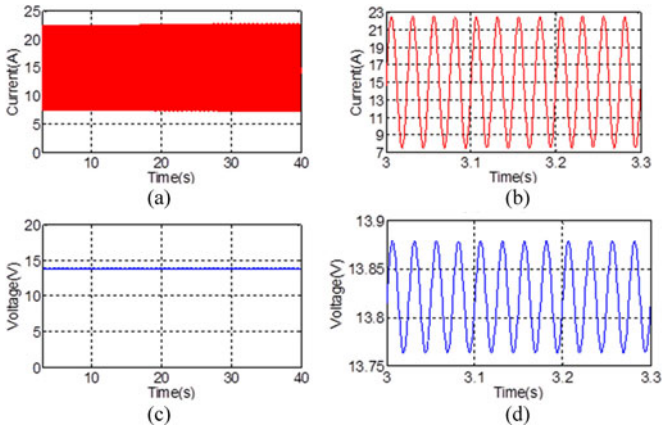

Fig. 11. Battery current and voltage: (a) battery current, (b) detail battery current, (c) battery voltage, and (d) detail battery voltage.

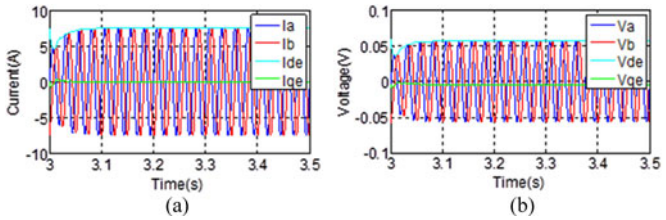

Fig. 12. d-q rotating coordinate system: (a) $\alpha\beta$ frame and d-q values of the ripple current, and (b) $\alpha\beta$ frame and d-q values of the ripple voltage.

carries out feedback control from the measured battery current and voltage; these values are used for online impedance measurement and the current and voltage controls are based on a PI controller. Typically, the dc current reference is determined by the *C*-rate of the battery.

By applying a *dq* transformation to the measured output values and several filters, the impedance and phase angle can be extracted [41]. The total impedance is

$$|Z_T| = \frac{\sqrt{v_q^2 + v_d^2}}{\sqrt{i_q^2 + i_d^2}}. \tag{14}$$

The active, reactive, and apparent powers are

$$P_{\text{ripple}} = \frac{(V_{qe}I_{qe} + V_{de}I_{de})}{2}, \quad Q_{\text{ripple}} = \frac{(V_{qe}I_{de} - V_{de}I_{qe})}{2}$$

$$S_{\text{ripple}} = \sqrt{P_{\text{ripple}}^2 + Q_{\text{ripple}}^2}. \tag{15}$$

The phase angle is

$$\theta = \cos^{-1}\left(\frac{P_{\text{ripple}}}{S_{\text{ripple}}}\right) \quad \text{or} \quad \theta = \tan^{-1}\frac{V_{qe}}{V_{de}}. \tag{16}$$

From theta, θ, and the total impedance, the real and imaginary parts of impedances can be obtained

$$Z_{\text{real}} = |Z_T|\cos\theta \quad \text{and} \quad Z_{\text{img}} = |Z_T|\sin\theta. \tag{17}$$

C. Optimal Frequency Tracking Control

Fig. 10 shows the state diagram of the optimal frequency tracking controller. In order to obtain the optimal frequency, the

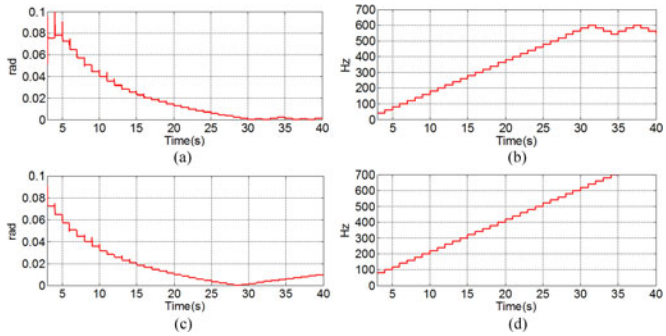

Fig. 13. Optimal frequency and frequency sweeping: (a) Radian change with optimal frequency control, (b) Optimal frequency point with optimal frequency control, (c) Radian change without optimal frequency control and (d) frequency without optimal frequency control.

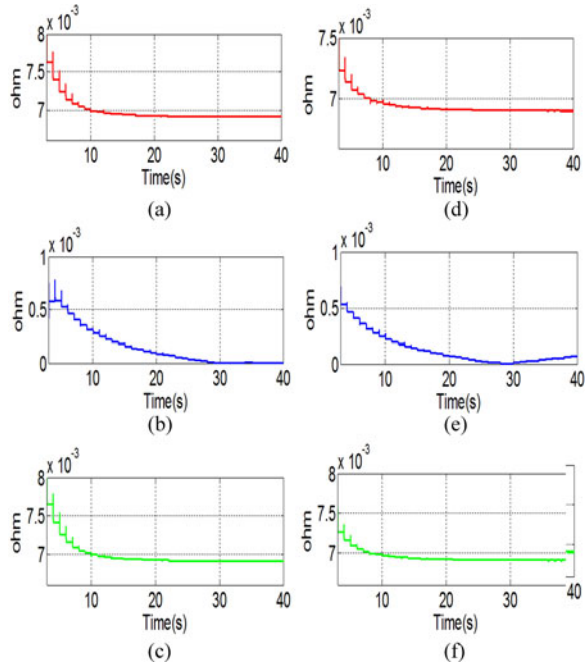

Fig. 14. The impedance values: (a) Real part of impedance with optimal frequency control, (b) Imaginary impedance with optimal frequency control, (c) Total impedance with optimal frequency control, (d) Real part of impedance without optimal frequency control , (e) Imaginary impedance without optimal frequency control and (f) Total impedance without optimal frequency control.

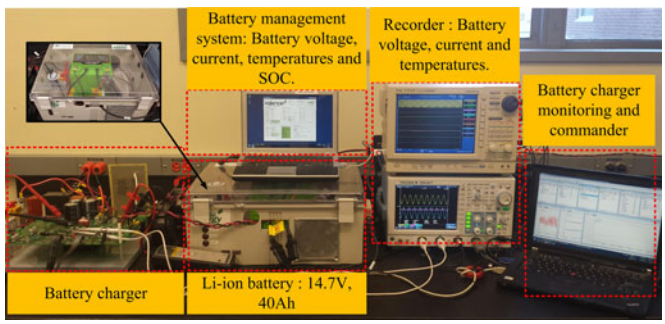

Fig. 15. Battery test bed.

TABLE I
PARAMETERS OF BATTERY CHARGER

	Parameter	Symbol	Value	Unit
Converter	Filter inductor	L_f	0.7	mH
	Filter capacitor	C_f	0.6	uF
	Filter cut-off frequency	f_c	7.78	kHz
	Switching frequency	f_s	20	kHz
	Input dc voltage	$V_{\rm in}$	50	V_{dc}
	Sampling time	$T_{\rm samp}$	50	us
Battery	Cable inductance	L_e	2.8	uH
	Electrolyte resistance or Ohmic resistance	R_o	6.9	mΩ
	Charge transfer resistor	$R_{\rm CT}$	1.2	mΩ
	Double-layer capacitance	$C_{\rm DL}$	2.65	F

Perturb and Observe method is applied, shown in Fig. 10(a). The optimal frequency is defined as

$$f_{\rm optimal} = f_{\rm optimal\_old} + f_{\rm perturbation}. \tag{18}$$

The imaginary part of impedance, $\mathrm{Im}|Z|$, and the perturbation of frequency can be controlled by

$$\mathrm{Im}|Z| = f(i, v)$$
$$\begin{cases} \mathrm{Im}\,|Z| > \mathrm{Im}\,|Z|_{\rm min}\ f_{\rm purtubation} = -f_{\rm min} \\ \mathrm{Im}\,|Z| < \mathrm{Im}\,|Z|_{\rm min}\ f_{\rm purtubation} = +f_{\rm min} \end{cases} \tag{19}$$

where $f_{\rm min}$ is 10 Hz and $\mathrm{Im}|Z|_{\rm min}$ can be defined by the range of maximum error in the impedance calculation.

As a result, the angular frequency is determined, $\omega_{\rm optimal} = 2\pi f_{\rm optimal}$. The battery current can be defined as

$$I_{\rm bat} = I_{C-\rm rate} + M\sin\left(\omega_{\rm optimal} t\right) \tag{20}$$

where *M* is the magnitude of the ac ripple current.

Based on this algorithm, impedance tracking is performed, as shown in Fig. 10(b). At the minimum imaginary impedance, the optimal frequency can be determined.

V. SIMULATION

In order to analyze the proposed algorithm, the parameters specified in Table I are used. L_e, R_O, $R_{\rm CT}$, and $C_{\rm DL}$ are measured using Model 1260 of Solartron analytical. A synchronous buck converter is adopted for the charger, and Simulink is used to verify the proposed method.

Ripple current generated for the impedance measurement is shown in Fig. 11. The battery current, $I_{\rm bat}$, and voltage, $V_{\rm bat}$, both contain a dc component and ac ripple component. In Fig. 11(a), $I_{\rm bat}$ is 15 $\mathrm{A_{dc}}$, superposed with a $\pm$7.5 $\mathrm{A_{ac}}$ ripple. A detailed view is shown in Fig. 11(b). When the current is injected, the ac component of the voltage response is $\pm$ 0.12 V, as shown in Fig. 11(c), and in greater detail in Fig. 11(d).

The *dq* transformation values, in response to changes in ripple frequency, are shown in Fig. 12(a). From this method, v_{dq} and i_{dq} values are obtained. v_d and i_d have peak values of v_α and i_α, respectively. v_q and i_q are vectors in the *q*-axis, which is orthogonal to the *d*-axis. Fig. 12(b) shows i_d, i_q, v_d, and v_q in detail. Dc components of these values are eliminated through the band-pass filter. In addition, the $\alpha\beta$ frame has 90° difference angles.

Fig. 13 shows the proposed optimal frequency tracking method. The radian values of the power angle theta, θ, is plotted with respect to changes in the ripple frequency by the Perturb and Observe method, shown in Fig. 13(a) and (b). It is demonstrated that in the region ($\sim$580 Hz) the θ is reduced to approximately zero, where both inductive and capacitive reactance are canceled. The proposed method maintains the ripple frequency around this point to maintain low- imaginary impedance. In Fig. 13(c) and (d), the frequency sweep continuously increases. The imaginary impedance over the range of the frequency sweep can be observed; below 580 Hz, the imaginary impedance is predominantly capacitive; at 580 Hz, the imaginary impedance is nearly zero and; above 580 Hz, the imaginary impedance is predominantly inductive.

Fig. 14 shows the change in impedance according to the changes in frequency. Fig. 14(a)–(c) demonstrates the impedance as a result of optimal ripple frequency control. At the optimal frequency point, the real and imaginary parts of impedances are minimized. Fig. 14(d)–(f) demonstrates the impedance as a result of an uncontrolled frequency sweep, which causes the imaginary part of impedance to increase after the optimal frequency point. Therefore, the total impedance has a minimum value around the optimal frequency point.

VI. EXPERIMENTAL RESULTS

In order to verify the proposed method, the battery test is performed under diverse test conditions. Fig. 15 shows the test bed. In the first section, the sinusoidal ripple current and impedance measurement performances are verified. Subsequently, in the second section, the detection of the beginning of activation polarization is verified. The third section demonstrates the optimal frequency tracking. Last section shows the overall experimental result based on these functions and algorithms. The charging performance is verified under several different conditions including varied sinusoidal ripple current frequency and magnitude conditions and the proposed method.

A. Sinusoidal Ripple Current According to Frequency Sweeping

Fig. 16 shows the frequency and magnitude of the ripple current. Fig. 16(a) shows the high-frequency ripple current, at $\pm$7.5 A at 600 Hz. In Fig. 16(b), the ripple frequency is 1 Hz. Fig. 16(c) shows the beginning of an ascending frequency sweep starting at 1 Hz. The battery voltage is plotted with respect to each ripple frequency, and it is observed that the optimal frequency reduces oscillations of the battery voltage most effectively.

B. Detecting the Saturation of Battery Impedance Value According to State of Charge (SOC)

Fig. 17 shows the real part of impedance value according to SOC. For this test, a ripple current of magnitude $\pm$1 A is applied. From these results, the beginning point of activa-

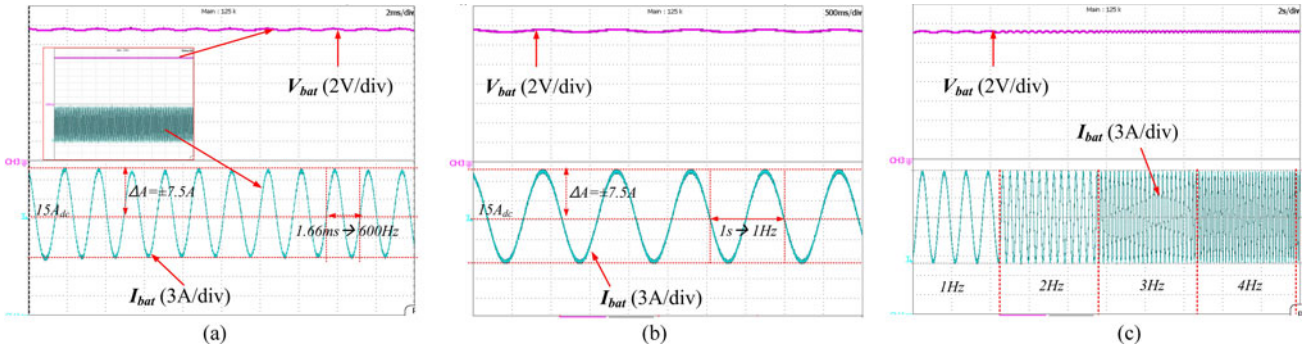

Fig. 16. Sinusoidal ripple current: (a) 600Hz, ±7.5A, (b) 1Hz, ±7.5A and (c) frequency sweeping.

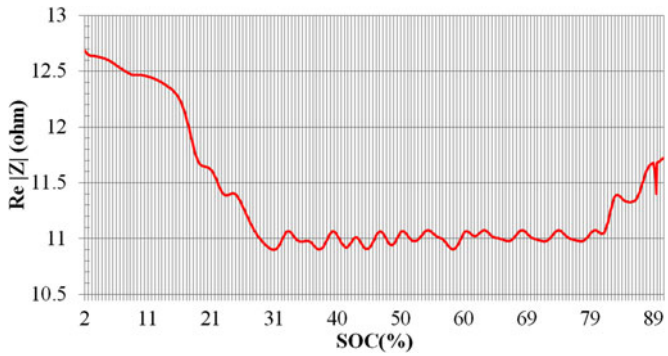

Fig. 17. Real part of the impedance of the battery according to SOC.

tion polarization is determined. At around 31% SOC, the real part of impedance becomes saturated, meaning that activation polarization due to the double-layer capacitance and charge transfer reaction begins.

C. Optimal Frequency Tracking

Fig. 18 shows the experimental results of the proposed tracking method for determining the optimal ripple frequency. The impedance variations of the imaginary and real parts according to the frequency sweep are investigated. At 410 Hz, the imaginary impedance is minimized. At 560 Hz the impedance begins to increase, shown in Fig. 18(a). This means that this frequency range is the boundary between predominant capacitance and inductance. At this boundary, the real part of impedance approaches a minimum value, shown in Fig. 18(b).

The proposed algorithm, based on the Perturb and Observe algorithm is performed, shown in Fig. 18(c) and (d). At the boundary condition, the imaginary impedance is minimized and the frequency cycles through several different values around this point, shown in Fig. 18(c). As a result, the real part of impedance approaches a minimum value, shown in Fig. 18(d).

D. Comparison of Charging Methods

The following section details the impacts of ripple current frequency and magnitude on battery charging efficiency. The first case study investigates the impacts of frequency, and the latter case study investigates the impacts of magnitude.

The first case study is to investigate the impact of ripple current frequency over several hundred hertz as follows:

1) CCCV;
2) low frequency (1 Hz, 10 Hz);
3) moderate frequency effect (50 Hz);
4) between moderate frequency and optimal frequency (100 Hz and 300 Hz);
5) around optimal frequency effect and more high-frequency range (400 Hz, 500 Hz, and 600 Hz).

Test purpose of low-frequency ripple current is to verify an impact of high real part of impedance of the battery. Moderate frequency is boundary condition to solve lithium plating. Tests from 100 to 300 Hz is to show the increased efficiency with respect to the increased frequencies. 400 and 500 Hz are around optimal frequency. 600 Hz is the frequency range with inductive component. From results of these test conditions, the proposed method is verified and detail test condition and results shown in Table II.

Test 1, CCCV, result shows long charging time, low efficiency, and high temperature, because lithium plating has not been solved compare to other test results. Low frequency cases, which have tests 2 and 3, show similar results as CCCV. Test 4, 50 Hz, shows the result of moderate frequency of R_{CT} and C_{DL}. The efficiency is increased compare to CCCV. Tests 5 and 6 show the frequency impact. The more the frequency is increased, the efficiency is improved. Tests 7, 8, and 9 have a purpose for investigation regarding optimal frequency and frequency of inductive range. As a result, the efficiency is best at 400 Hz because this frequency range closes the optimal frequency. The more a frequency is increased, the more efficiency becomes worse compared to 400 Hz. This is because the total impedance of the battery goes to an inductive range. Based on these tests and Test 6, the proposed method is verified. In the proposed method, the optimal frequency range is from 410 to 550 Hz shown in Fig. 19. As applying the proposed method, it shows faster charging and higher efficiency than 400 Hz result. The results show that the charging time and efficiency of the proposed method are improved up to 5.1% and 5.6%, respectively, compared to CCCV. Note that the efficiency is calculated as follows:

$$\eta = \frac{\int_0^{T_{\mathrm{charge\_end}}} i_{\mathrm{bat\_discharging}}\, dt}{\int_0^{T_{\mathrm{discharge\_end}}} i_{\mathrm{bat\_charging}}\, dt} \times 100[\%]. \qquad (21)$$

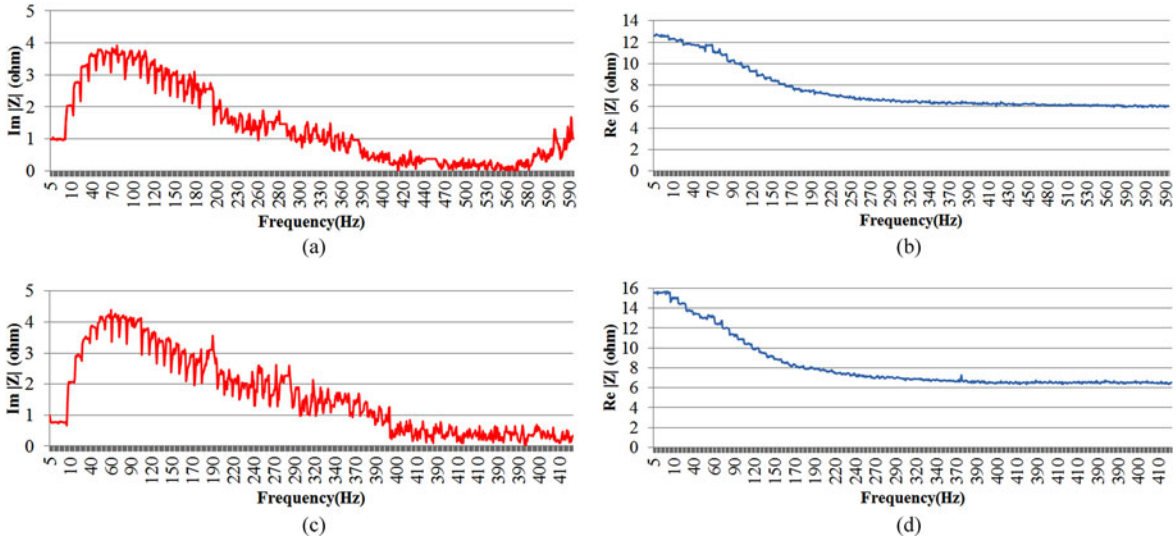

Fig. 18. Optimal frequency control: (a) imaginary impedance with no control, (b) real part of impedance with no control, (c) imaginary impedance with optimal frequency control and (d) real part of impedance with optimal frequency control.

TABLE II
FREQUENCY IMPACT OF RIPPLE CURRENT

	Charging Frequency (Hz)	Charging Current (A)	Charging time (min)	Discharging time (min)	Charging T_{max} (°C)	Discharging T_{max} (°C)	Efficiency (%)
Test 1	CCCV	15 A_{dc}	173.8	108.1	31.1	31.7	93.3
Test 2	1 Hz	15 A_{dc} + 7.5 A_{ac}	173.9	112.1	29.8	32.6	93.8
Test 3	10 Hz	15 A_{dc} + 7.5 A_{ac}	173.2	112.2	28.8	32.0	93.7
Test 4	50 Hz	15 A_{dc} + 7.5 A_{ac}	173.1	112.9	29.6	31.8	94.7
Test 5	100 Hz	15 A_{dc} + 7.5 A_{ac}	172.8	113.0	31.4	31.8	95.4
Test 6	300 Hz	15 A_{dc} + 7.5 A_{ac}	170.5	113.7	29.0	32.1	96.4
Test 7	400 Hz	15 A_{dc} + 7.5 A_{ac}	167.7	114.4	29.1	31.9	97.8
Test 8	500 Hz	15A_{dc} + 7.5 A_{ac}	170.1	113.4	28.5	32.1	96.2
Test 9	600 Hz	15 A_{dc} + 7.5 A_{ac}	172.4	112.7	29.8	31.4	94.0
Test 10	***Optimal***	15 A_{dc} + 7.5 A_{ac}	***164.9***	***114.7***	29.3	32.4	***98.9***

TABLE III
MAGNITUDE IMPACT OF RIPPLE CURRENT

	Charging Frequency (Hz)	Charging Current (A)	Charging time (min)	Discharging time (min)	Charging T_{max} (°C)	Discharging T_{max} (°C)	Efficiency (%)
Test 11	CCCV	10 A	255.4	112.7	27.9	33.5	96.1
Test 12	Optimal	10 A_{dc} +1 A_{ac}	250.8	118.8	27.3	33.2	97.2
Test 13	Optimal	10 A_{dc} + 10 A_{ac}	252.5	119.1	28.5	32.7	97.5
Test 14	Optimal	10 A_{dc} + 7.5 A_{ac}	***246.8***	119.2	28.3	32.1	97.2

Fig. 19(a) demonstrates the current profiles of the proposed method under all conditions. When the battery reaches 26% SOC, the magnitude of the ripple current is changed from ±1 to ±7.5 A. As a result, the last charging phase of the proposed method is faster than the other charging method. In addition, in Fig. 19(b), the voltage of the proposed method reaches the maximum allowable voltage faster than the other charging method. In addition, during charging, the temperatures of all charging methods, except CCCV remain below the CCCV temperature by approximately 1 °C to 2 °C, shown in Fig. 19(c). Intuitively, the differences of efficiency values of each method varied in improvements of about 3% to 5%, when compared to CCCV and sinusoidal ripple current charging. Through the charging results, the proposed method is verified. However, to clarify further, a discharging test is required, shown in Fig. 20. The discharging tests are performed under the same CC discharging. 20 A_{dc} of discharging current is applied and is a 0.5C-rate. The proposed method and sinusoidal ripple current charging with diverse frequencies have increased discharging time, compared to CCCV, shown in Fig. 20(a). In addition, the discharge temperatures of CCCV and the 1-Hz ripple current have the highest tempera-

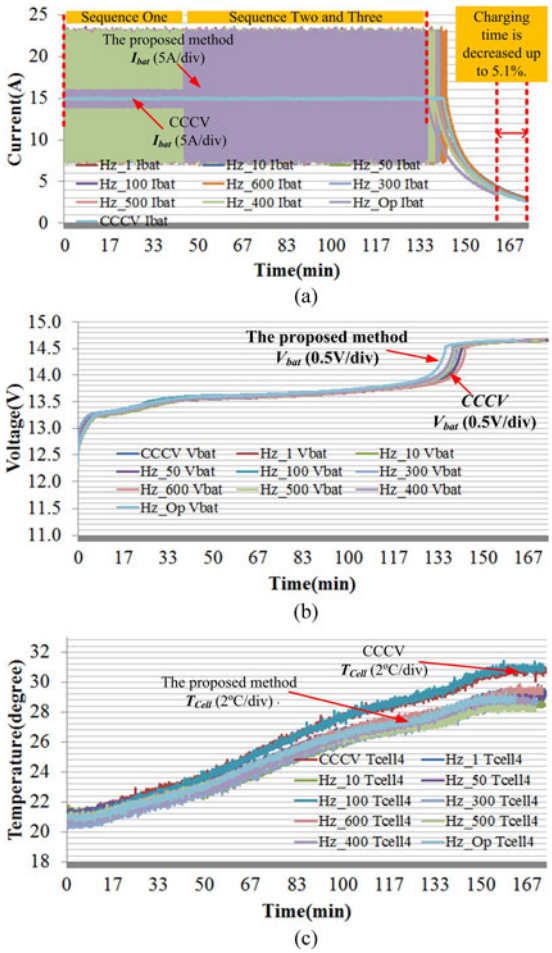

Fig. 19. Charging results: (a) charging current profiles, (b) battery voltage profiles and (c) temperatures.

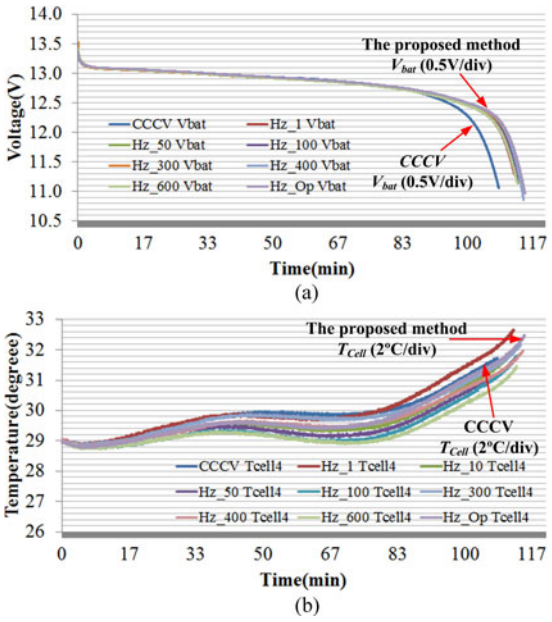

Fig. 20. Discharging results: (a) Discharging voltage curves and (b) temperatures.

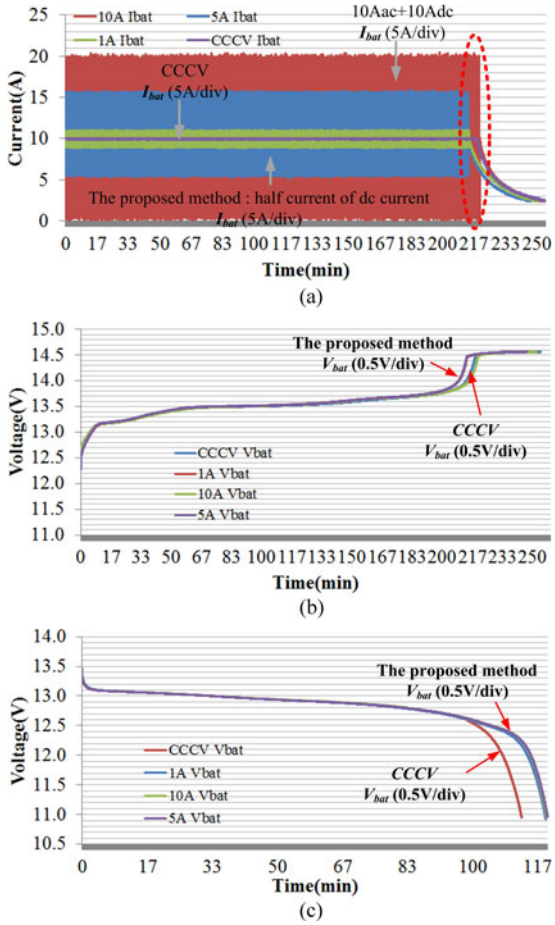

Fig. 21. Impact of magnitudes of ripple current: (a) Charging current profiles, (b) battery voltage profiles, and (c) battery voltage discharge profiles.

ture value amongst all charging methods, shown in Fig. 20(b). Conclusively, the proposed method has the highest efficiency, longest discharging time, and fastest charging time.

The second case study is to verify the effects of various magnitudes of ripple current. In this paper, the proposed magnitude of the peak to peak ripple current should be half of the magnitude of the dc current. In order to analyze the impacts of various ripple current magnitudes, the minimum magnitude, maximum magnitude, CCCV, and the proposed value are used, and the test methods are as follows:

Table III and Fig. 21 show the results of magnitude impact of the charging current. The shortest charging time is taken by the proposed method of Test 14. Most discharging times are similar except CCCV of Test 11. Therefore, for sinusoidal current charging, it was verified that the excessively high-peak current is not necessary. From these results, a charging scheme design guide is created and its benefits are that the charger can provide a small peak current.

VII. Conclusion

This paper presents an advanced sinusoidal ripple current charging algorithm based on an embedded impedance measurement. This paper performs rigorous analysis of electrochemical

characteristics and uses them as a basis for a sinusoidal ripple current charging algorithm to minimize variations of charge transfer impedance. To obtain the optimal ripple current frequency, ac impedance analysis based on the *dq* transformation method is used. This method results in improved charging efficiency, reduced activation polarization, and reduced Lithium plating. Furthermore, this paper verified the frequency and magnitude of ripple current under diverse test conditions alongside the proposed method. Based on these test results, the charging time and efficiency of the proposed method are improved by 5.1% and 5.6%, respectively.

In addition, conventional sinusoidal charging methods are focused on minimizing the imaginary component of the impedance. In this case, the charging current control parameter is frequency dependent; however, it does not take into account time-dependent characteristics during charging. Typically, lithium plating does not occur in the early stages of charging. In other words, an advanced charging algorithm requires controllability according to the time-varying electrochemical state, as well as the imaginary component of the impedance. In addition, conventional sinusoidal charging methods do not take into account the magnitude of the ripple current. The ripple magnitude is an important consideration when designing a battery charger, because peak current affects charger component specifications and operation.

REFERENCES

[1] D. Anseán, M. González, J. C. Viera, V. M. García, C. Blanco, and M. Valledor, "Fast charging technique for high power lithium iron phosphate batteries: A cycle life analysis," *J. Power Sources*, vol. 239, pp. 9–15, Oct. 2013.

[2] M. Ecker, N. Nieto, S. Käbitz, J. Schmalstieg, H. Blanke, A. Warnecke, and D. U. Sauer, "Calendar and cycle life study of Li(NiMnCo)O2-based 18650 lithium-ion batteries," *J. Power Sources*, vol. 248, pp. 839–851, Feb. 2014.

[3] P. Verma, P. Maire, and P. Novák, "A review of the features and analyses of the solid electrolyte interphase in Li-ion batteries," *Electrochimica Acta*, vol. 55, no. 22, pp. 6332–6341, Sep. 2010.

[4] A. Patil, V. Patil, D. Wook Shin, J.-W. Choi, D.-S. Paik, and S.-J. Yoon, "Issue and challenges facing rechargeable thin film lithium batteries," *Mater. Res. Bull.*, vol. 43, nos. 8/9, pp. 1913–1942, Aug./Sep. 2008.

[5] M. Park, X. Zhang, M. Chung, G. B. Less, and A. M. Sastry, "A review of conduction phenomena in Li-ion batteries," *J. Power Sources*, vol. 195, no. 24, pp. 7904–7929, Dec. 2010.

[6] B. K. Purushothaman and U. Landau, "Rapid charging of lithium-ion batteries using pulsed currents: A theoretical analysis," *J. Electrochem. Soc.*, vol. 153, no. 3, pp. A533–A542, 2006.

[7] S. S. Zhang, "The effect of the charging protocol on the cycle life of a Li-ion battery," *J. Power Sources*, vol. 161, no. 2, pp. 1385–1391, Oct. 2006.

[8] S. S. Zhang, K. Xu, and T. R. Jow, "Study of the charging process of a LiCoO2-based Li-ion battery," *J. Power Sources*, vol. 160, no. 2, pp. 1349–1354, Oct. 2006.

[9] S. S. Zhang, K. Xu, and T. R. Jow, "Electrochemical impedance study on the low temperature of Li-ion batteries," *Electrochimica Acta*, vol. 49, no. 7, pp. 1057–1061, Mar. 2004.

[10] B. K. Purushothaman, P. W. Morrison Jr., and U. Landau, "Reducing mass-transport limitations by application of special pulsed current modes," *J. Electrochem. Soc.*, vol. 152, no. 4, pp. J33–J39, 2005.

[11] D. Linden, *Handbook of batteries*, 3rd ed. New York, NY, USA: McGraw-Hill, 2002.

[12] A. Kirchev, A. Delaille, F. Karoui, M. Perrin, E. Lemaire, and F. Mattera, "Studies of the pulse charge of lead-acid batteries for PV applications: Part III. Electrolyte concentration effects on the electrochemical performance of the positive plate," *J. Power Sources*, vol. 179, no. 2, pp. 808–818, May 2008.

[13] H. Zhang and M.-Y. Chow, "Comprehensive dynamic battery modeling for PHEV applications," in *Proc. IEEE Power Energy Soc. Gen. Meet.*, Jul. 2010, pp. 1–6.

[14] M. Zheng, B. Qi, and X. Du, "Dynamic model for characteristics of Li-ion battery on electric vehicle," in *Proc. IEEE 4th Conf. Ind. Electron. Appl.*, May 2009, pp. 2867–2871.

[15] A. Kirchev, A. Delaille, M. Perrin, E. Lemaire, and F. Mattera, "Studies of the pulse charge of lead-acid batteries for PV applications: Part II. Impedance of the positive plate revisited," *J. Power Sources*, vol. 170, no. 2, pp. 495–512, Jul. 2007.

[16] K. B. Chin, B. V. Ratnakumar, M. C. Smart, K. A. Smith, and S. Narayanan, "Evaluation of rapid charge methodologies for Li-ion chemistry," *ECS Trans.*, vol. 11, no. 29, pp. 43–53, 2008.

[17] L. T. Lam, H. Ozgun, O. V Lim, J. A. Hamilton, L. H. Vu, D. G. Vella, and D. A. J. Rand, "Pulsed-current charging of lead-acid batteries—A possible means for overcoming premature capacity loss?" *J. Power Sources*, vol. 53, pp. 215–228, 1995.

[18] H. J. Ploehn, P. Ramadass, and R. E. White, "Solvent diffusion model for aging of lithium-ion battery cells," *J. Electrochem. Soc.*, vol. 151, no. 3, pp. A456–A462, 2004.

[19] P. Petchjatuporn, N. Khaehintung, K. Sunat, P. Sirisuk, and W. Kiranon, "Implementation of GA-trained GRNN for Intelligent fast charger for Ni-Cd batteries," in *Proc. CES/IEEE 5th Int. Power Electron. Motion Control Conf.*, Aug. 2006, vol. 1, pp. 1–5.

[20] Y.-H. Liu and Y.-F. Luo, "Search for an optimal rapid-charging pattern for Li-ion batteries using the Taguchi approach," *IEEE Trans. Ind. Electron.*, vol. 57, no. 12, pp. 3963–3971, Dec. 2010.

[21] Y.-H. Liu, C.-H. Hsieh, and Y.-F. Luo, "Search for an optimal five-step charging pattern for Li-ion batteries using consecutive orthogonal arrays," *IEEE Trans. Energy Convers.*, vol. 26, no. 2, pp. 654–661, Jun. 2011.

[22] Y.-H. Liu, J.-H. Teng, and Y.-C. Lin, "Search for an optimal rapid charging pattern for lithium-ion batteries using ant colony system algorithm," *IEEE Trans. Ind. Electron.*, vol. 52, no. 5, pp. 1328–1336, Oct. 2005.

[23] A. Khosla, S. Kumar, and K. K. Aggarwal, "Fuzzy controller for rapid nickel-cadmium batteries charger through adaptive neuro-fuzzy inference system (ANFIS) architecture," in *Proc. 22nd Int. Conf. North Amer. Fuzzy Inf. Process. Soc.*, Jul. 2003, pp. 540–544.

[24] J. Yan, G. Xu, H. Qian, and Y. Xu, "Battery fast charging strategy based on model predictive control," in *Proc. IEEE 72nd Veh. Technol. Conf. Fall*, Sep. 2010, pp. 1–8.

[25] L.-R. Chen, "A design of an optimal battery pulse charge system by frequency-varied technique," *IEEE Trans. Ind. Electron.*, vol. 54, no. 1, pp. 398–405, Feb. 2007.

[26] L.-R. Chen, "Design of duty-varied voltage pulse charger for improving Li-ion battery-charging response," *IEEE Trans. Ind. Electron.*, vol. 56, no. 2, pp. 480–487, Feb. 2009.

[27] L.-R. Chen, S.-L. Wu, D.-T. Shieh, and T.-R. Chen, "Sinusoidal-ripple-current charging strategy and optimal charging frequency study for Li-Ion batteries," *IEEE Trans. Ind. Electron.*, vol. 60, no. 1, pp. 88–97, Jan. 2013.

[28] F. Lacressonniere, B. Cassoret, and J.-F. Brudny, "Influence of a charging current with a sinusoidal perturbation on the performance of a lead-acid battery," *IEE Proc. Electric Power Appl.*, vol. 152, no. 5, pp. 1365–1370, Sep. 2005.

[29] P. H. L. Notten, J. H. G. Op het Veld, and J. R. G. van Beek, "Boostcharging Li-ion batteries: A challenging new charging concept," *J. Power Sources*, vol. 145, no. 1, pp. 89–94, Jul. 2005.

[30] L.-R. Chen, R. C. Hsu, and C.-S. Liu, "A design of a grey-predicted Li-Ion battery charge system," *IEEE Trans. Ind. Electron.*, vol. 55, no. 10, pp. 3692–3701, Oct. 2008.

[31] C.-H. Lin, C.-Y. Hsieh, and K.-H. Chen, "A Li-Ion battery charger with smooth control circuit and built-in resistance compensator for achieving stable and fast charging," *IEEE Trans. Circuits Syst I, Reg. Papers*, vol. 57, no. 2, pp. 506–517, Feb. 2010.

[32] S. C. Kim and W. H. Hong, "Fast-charging of a lead–acid cell: Effect of rest period and depolarization pulse," *J. Power Sources*, vol. 89, no. 1, pp. 93–101, Jul. 2000.

[33] A. Kirchev, M. Perrin, E. Lemaire, F. Karoui, and F. Mattera, "Studies of the pulse charge of lead-acid batteries for PV applications: Part I. Factors influencing the mechanism of the pulse charge of the positive plate," *J. Power Sources*, vol. 177, no. 1, pp. 217–225, Feb. 2008.

[34] P. E. de Jongh and P. H. L. Notten, "Effect of current pulses on lithium intercalation batteries," *Solid State Ionics*, vol. 148, nos. 3/4, pp. 259–268, Jun. 2002.

[35] A. Jossen, "Fundamentals of battery dynamics," *J. Power Sources*, vol. 154, no. 2, pp. 530–538, Mar. 2006.
[36] J. Hong and C. Wang, "Kinetic behavior of $LiFeMgPO_4$ cathodematerial for Li-ion batteries," *J. Power Sources*, vol. 162, no. 2, pp. 1289–1296, Nov. 2006.
[37] C. W. Tanner, K. Z. Fung, and A. V. Virkar, "Comment on the effect of porous composite electrode structure on solid oxide fuel cell performance," *J. Electrochem.*, vol. 144, no. 1, pp. 21–30, 1997.
[38] E. M. Conte, F. V. Kral, and C. Fleig J., "Comparison, selection, and parameterization of electrical battery models for automotive applications," *IEEE Trans. Power Electron.*, vol. 28, no. 3, pp. 1429–1437, Mar. 2013.
[39] J. Niu, B. E. Conway, and W. G. Pell, "Comparative studies of self-discharge by potential decay and float-current measurements at C double-layer capacitor and battery electrodes," *J. Power Sources*, vol. 135, nos. 1/2, pp. 332–343, Sep. 2004.
[40] J. Niu, W. G. Pell, and B. E. Conway, "Requirements for performance characterization of c double-layer supercapacitors: Applications to a high specific-area c-cloth material," *J. Power Sources*, vol. 156, no. 2, pp. 725–740, Jun. 2006.
[41] Y.-D. Lee, S.-Y. Park, and S.-B. Han, "On-line optimal ion conductivity control of Li-ion battery," in *Proc. IEEE Energy Convers. Congr. Expo.*, Sep. 2012, pp. 4493–4500.

Yong-Duk Lee (S'06) received the B.S. degree in electronic engineering and the M.S. degree in electrical engineering from Hankyong National University, Anseong, Korea, in 2006 and 2008, respectively. Since 2011, he has been working toward the Ph.D. degree in power electronics at the University of Connecticut, Storrs, CT, USA.

From 2007 to 2010, he was an Associate Researcher with POSCO ICT.

Sung-Yeul Park (S'04–M'09) received the M.S. and Ph.D. degrees in electrical and computer engineering from Virginia Polytechnic Institute and State University (Virginia Tech), Blacksburg, VA, USA, in 2004 and 2009, respectively.

From 2002 to 2004, he was a Graduate Research Assistant with the Center for Rapid Transit Systems, Virginia Tech. From 2004 to 2009, he was a Graduate Research Assistant with the Future Energy Electronics Center, Virginia Tech. He joined the University of Connecticut, Storrs, CT, USA, as an Assistant Professor in the Department of Electrical and Computer Engineering and as an Associate Member of the Center for Clean Energy Engineering in 2009. His research interests include energy-efficient energy and power conversion, renewable and distributed generation integration, smart buildings, and microgrid applications.

Dr. Park received several international paper awards including a third paper award at the *IEEE Industry Applications Society Annual Meeting* in 2004, a best paper award at the *IEEE Power Conversion Conference* in 2007, an outstanding writing award in the International Future Energy Challenge in 2007, and a Torgersen Research Excellence Award from the College of Engineering, Virginia Tech, in 2009.